COBEM 2023 27TH INTERNATIONAL CONGRESS OF MECHANICAL ENGENEERING

ABCM Brazilian Society of Mechanical Sciences and Engineering
27th ABCM International Congress of Mechanical Engineering
December 04-08, 2023, Florianópolis-SC, Brazil

COB-2023-2304
IMPROVED HEALTH INDICATOR FOR LOW-SPEED BEARING DIAGNOSIS

Thiago Barroso Costa, thiago.costa@tucurui.ufpa.br
João Lucas Lobato Soares, soaresjoao974@gmail.com
Elton Prestes Souza, elton.souza@tucurui.ufpa.br
Jonatas Cruz da Silva, jonatas.cruz.silva@tucurui.ufpa.br
Walter dos Santos Sousa, wss@ufpa.br
Alexandre Luiz Amarante Mesquita, alexmesq@ufpa.br
André Luiz Amarante Mesquita, andream@ufpa.br
Federal University of Pará, Av. Brasília, s/n - Vila Permanente - 68.455-901 - Tucuruí, PA

Danilo de Souza Braga, danilo@dynamox.net
Dynamox, Rod. SC 401, km 01, nº 600, Rua Parque Tecnológico Alfa, Florianópolis - SC, 88030-909

Abstract. *Vibration analysis and acoustic emission have been useful for condition monitoring and fault detection and diagnosis of low-speed slew bearings. Nevertheless, the use of vibration signal is a challenge due to low-speed bearings operate subjected to large loads and sometimes non-stationary condition. Moreover, the weak fault bearing signal can be smeared/masked by noise from other sources. Hence, processing signal tools and machine learning algorithms has been proposed to address those issues. Non-linear features have presented satisfactory results for condition monitoring and fault diagnosis of low-speed slew bearings. Among non-linear features, the maximal Lyapunov exponent (MLE) has showed clearer outcomes for low-speed slew bearing fault detection and prognosis. The Lyapunov exponent characterizes the rate of separation of infinitesimally close trajectories in phase-space. Since 1993, when the current method was proposed, the distance between those trajectories has been measured based on Euclidean distance. Aiming to enhance class separation, this work proposes the use of Pearson and Spearman distances as novel means to find the nearest trajectories improving MLE separability of classes. The Welch t test statistic value was used as a comparative index which is based on predictors' separability. The methods were validated using vibration data from a controlled rotor test rig at shaft speed of 60 rpm, where healthy and damaged rolling bearings were tested. Finally, the results showed both Pearson and Spearman distances performed larger class separability, demonstrating that they can improve machine learning algorithm accomplishment for classification tasks.*

Keywords: *low-speed bearing fault diagnosis, largest Lyapunov exponent, Pearson distance, Spearman distance, Welch t test, machine learning*

1. INTRODUCTION

Most of the rotating machinery used in the industry operates by means of bearings which are the main causes of failure in rotating machinery. Faults on bearings can occur for many different reasons including fatigue, cracks, fractures, wear, improper mounting, corrosion, erosion, poor lubrication and plastic deformations, which can affect different parts as inner race, outer race and rolling elements. To avoid downtime and increase reliability, early fault detection in rotating machinery has been the interest of many researchers. Thus, there is a need for non-destructive techniques for monitoring, fault detection, diagnosis and prognosis of bearings. The most successful methods are currently based on analysis of vibration signals (Soleimani and Khadem, 2015). A normal bearing vibrates due to the variation of contact forces acting between the rolling elements and the raceways. The vibration characteristics of the bearing depend on the rotational speed, clearance, radial/axial load, rolling element stiffness, surface waviness and development of failure modes (Ghafari et al., 2008). By comparing the signals of a machine running in normal and faulty conditions, detection of incipient faults is possible, reducing the possibility of catastrophic damage and scheduling the downtime (Xinmin et al., 2007).

Considering the inherent shortcomings of time domain, frequency domain and time-frequency domain approaches to vibration data analysis, studies in dynamical systems and chaos theory have led to new types of signal models based on reconstructed phase spaces. The nonlinear approach as signal processing technique has been widely used in mechanics fault detection and diagnosis applications (Xinmin et al., 2007). Bearings contain localized faults that affect the chaotic characteristics of the vibration signals acquired from them. Lyapunov exponents (LEs) as mathematic representation are used to measure chaos in dynamical systems. As such, the associated LEs tend to change as the bearing advances from healthy to faulty states (Rai and Kim, 2020). Moreover, LEs are commonly applied to temporal series analysis of different fields including EEG analysis (Yakovleva et al., 2020), gait biomechanics analysis (Raffalt et al., 2019), financial market

(Ogunjo et al., 2021), structural and mechanism analysis (Awrejcewicz et al., 2017; Yousuf, 2019) and heart rate variability (Tayel and AlSaba, 2015).

The LEs have been exploited using experimental vibration signals acquired from regular rolling element bearings at relatively high rotation speed. Xinmin et al. (2007) proposed a novel approach based on Gaussian Mixture Models (GMM) and Bayesian Classifier with the largest Lyapunov exponent (LLE) and Lyapunov exponent spectrum entropy as classification features. The authors found good results and observed that the application of the isolated LLE fails to accurately separate the ball and outer vibration signals in the bearing fault diagnosis applications. Qingjun and Yang (2019) also investigated the effective of LLE for bearing fault diagnosis reporting that the LLE of the vibration signal of outer ring faults was slightly larger than that of inner ring faults. Additionally, the LLE value of the vibration signal under normal working conditions was relatively small.

Rai and Kim (2020) presented a novel approach to prognose the degradation and estimate the RUL (remaining useful life) of bearings based on vibration analysis, LLE, a probabilistic-self organizing map (p-SOM), and the Gini-Simpson (GS) index. Soleimani and Khadem (2015) developed a chaotic feature space including approximate entropy (ApEn), correlation dimension (CD), and LLE achieving accurate ball bearing and gearbox faults classifications through artificial neural network (ANN) algorithm. According to Patel et al. (2012), state change was identified using the phase space trajectories and LEs of Duffing equation allowing detection of local defects existing on races of deep groove ball bearing in the presence of external vibrations. Ghafari et al. (2008) studied the effect of localized defects on chaotic vibration of bearings and concluded that the chaotic measures such as CD and LEs are capable of detecting bearing defects.

Nevertheless, bearings operating at low speed have vibration signal of low energy and fault information can be masked by strong background noise interference, which can make traditional diagnostic methods and time and/or frequency domain features inefficient to fault detection task. Low-speed bearings are commonly used in large industrial machineries such as turntables, steel mill cranes, off-shore cranes, rotatable trolleys, excavators, reclaimers, stackers, swing shovels, sludge thickeners, belt conveyors and wind turbines (Caesarendra et al., 2015). The LLE was applied by Caesarendra et al. (2015) for the first time to detect changes in the conditions of low-speed slew bearings and the authors concluded that the LLE tracked bearing degradation better than traditional features such as RMS, high-order statistics, and time-frequency approaches including empirical mode decomposition (EMD) and wavelet decomposition. Wang et al. (2018) proposed a combined failure diagnosis method based on maximum correlated kurtosis deconvolution (MCKD) algorithm, complementary ensemble empirical mode decomposition (CEEMD) and nonlinear features including LLE, ApEn, CD and sample entropy (SE) for large-size and heavy-load slewing bearings, reaching high accuracies with support vector machine (SVM) classification algorithm.

Additionally, both aforementioned researches relative to low-speed bearing calculated the LLE using the algorithm proposed by Rosenstein et al. (1993). The main highlights of Rosenstein's approach are computation cost reduction and its applicability to relatively small data. Rosenstein's algorithm calculates the LLE first reconstructing an appropriate state space using the experimental time series through the method of delay. Then, the distance between two neighboring points (i.e., initial conditions) of the state space is measured and tracked over the entire evolution time of the system. A revision to the Rosenstein's method was firstly proposed in 2019 by Mehdizadeh (2019) in order to make the numerical algorithm be more robust to noise. The aim was investigating the effect of increasing number of initial neighboring points on the LLE value and compare to values obtained by filtering simulated and experimental time series. The presence of noise using experimental time series could have adverse effects on the calculated LLE since it increases the possibility of picking false neighbors in the state space and thus computation of inconsistent LLE values (Mehdizadeh and Sanjari, 2017).

Once the original Rosenstein's method consists of finding neighboring points in phase space using Euclidean norm, this paper aims investigating whether the use of other distance metrics in finding neighboring points stage can improve class separability of LLE as health indicator. In machine learning classification task, the use of predictors that can enhance the differences between classes can make the machine learning algorithm more robust and generalized. Hence, the Pearson and Spearman distances were applied to find the initial neighboring point for each reference point of the trajectory. For this purpose, vibration data from testing rolling element bearing was acquired at low speed of 60 rpm, collecting data for healthy and faulty conditions. Moreover, after the calculation of LLE computed with the three different metrics (Euclidean, Pearson and Spearman), the separability significance was compared using the t-Welch statistic value, which compares the sample mean and the sample variance of both classes. Finally, the application of Pearson and Spearman distance presented superior class separability compared with Euclidean distance-based Rosenstein's approach.

2. ROSENSTEIN'S METHOD-BASED LLE ALGORITHM

Lyapunov exponent (LE) is one of the commonly used methods for determining the degree of chaoticity. The key characteristic of chaotic trajectories in phase space dynamical system is their sensitivity to the initial conditions. When an attractor is chaotic, The LE is a quantitative measure of the sensitive dependence on the initial conditions. The LE gives the rate of exponential divergence from perturbed initial conditions. It is the average rate of divergence (or convergence) of two neighboring trajectories. The system with positive exponents has a chaotic characteristic as trajectories that are initially close together move apart over time being generally described by a strange attractor. Actually,

there is a whole spectrum of LEs. Their number is equal to the dimension of the phase space. Furthermore, in many applications it is sufficient to estimate only the largest value of the Lyapunov spectrum (Patel et al., 2012; Xinmin et al., 2007).

In order to estimate the LLE reconstructing phase space of the dynamical system is needed. It is possible to reconstruct the attractor in an *m*-dimensional state space based on a time series $\{x_1, x_2, \cdots, x_N\}$, because transients signals can be considered as outputs of chaotic dynamical system. The attractor of a dynamical system can be easily obtained if the differential equations for the relevant variables of the system are known. However, for most of the experimental signals, a prior information about the underlying strange attractor is not known. Thus, extra effort to reconstruct the strange attractor from a time series is required. For this purpose, the time delay method and the embedding dimensional theorem proposed by Takens (1981) are used. In the method of time delays, the attractor is embedded in an *m*-dimensional space and the *m*-dimensional matrix is constructed from the original time series $\{x_1, x_2, \cdots, x_N\}$ as seen in Eq. 1. (Xinmin et al., 2007). The objective of the reconstruction is to find a *m*-dimensional space so that the trajectories describe the attractor, and each point of that trajectory is a vector of the aforementioned *m*-dimensional matrix and represents a state of the system. There are several methods to select the embedding dimension, but the most common method is the false nearest neighbors (FNN) approach. For choosing the time delay, the method of mutual information is appropriate for nonlinear signals (Soleimani and Khadem, 2015).

$$\boldsymbol{X} = \begin{Bmatrix} x_1 & x_{1+J} & x_{1+2J} & \cdots & x_{1+(m-1)J} \\ x_2 & x_{2+J} & x_{2+2J} & \cdots & x_{2+(m-1)J} \\ x_3 & x_{3+J} & x_{3+2J} & \cdots & x_{3+(m-1)J} \\ \vdots & \vdots & \vdots & \ddots & \vdots \\ x_M & x_{M+J} & x_{M+2J} & \cdots & x_{M+(m-1)J} \end{Bmatrix}, \tag{1}$$

Above, $\boldsymbol{X}$ represents a generalized state space matrix which is derived from the original time series $\{x_1, x_2, \cdots, x_N\}$ subjected to embedding dimension method and time delay. Once delay J and embedding dimension m are determined, and the size of the time series N is known, the relation between these variables and the number of reconstructed vectors M can be calculated in the following way: $M = N - (m-1)J$ (Caesarendra et al., 2015). According to Rosenstein's approach, after phase space reconstruction it is required to find the nearest point for each row (state) of the phase space matrix. For this purpose, Equation 2 calculates the distance $d_j(0)$ between *nth*-nearest neighbor, $\boldsymbol{X}_j$, to the reference point $\boldsymbol{X}_{\hat{\jmath}}$, where $\|.\|$ denotes Euclidean distance.

$$d_j(0) = \min_{\boldsymbol{X}_{\hat{\jmath}}} \left\| \boldsymbol{X}_j - \boldsymbol{X}_{\hat{\jmath}} \right\|, \tag{2}$$

The equation above is subjected to the constraint that nearest neighbors have a temporal separation greater than the mean period of the time series. For Mehdizadeh (2019), the constraint considers distances greater than mean period in order to avoid picking points of same trajectory. Analytically, that means $|j - \hat{\jmath}| > \mu$, and μ is called the mean period, which is estimated by Eq. 3, where f_s is sampling rate, $\bar{f_p}$ is the mean normalized frequency of the power spectrum ($\bar{f_p}$ can also be the median frequency of the magnitude spectrum), and $\lceil . \rceil$ represents a ceil function.

$$\mu = \lceil f_s / \bar{f_p} \rceil, \tag{3}$$

Then, the LLE is estimated as the mean rate of separation of the nearest neighbors. Caesarendra's algorithm utilized the method of *k*-iteration to improve the accuracy of the measured distance. Finally, the iteration is limited to $|M - k| \geq j$, and the LLE is accurately computed using a least-square fit equation described by Eq. 3 based on average separation. Where k assumes successively all values between the Expansion Range from k_{min} to k_{max}.

$$LLE(k) = \frac{f_s}{M-k} \sum_{j=1}^{M-k} \ln \boldsymbol{d_j}(k), \tag{4}$$

Figure 1 shows the flowchart since vibration data acquisition to initial distance matrix obtaining. In order to illustrate main steps, a time series with 9 elements, $N = 9$, was used. Moreover, the state space reconstruction (just as an example) was made with $J = 2$ and $m = 4$ (then $M = 3$). The dashed square performs the iteration process $i = \{1, 2, \ldots, M\}$, such that $i = 1$ is used as an example in Fig. 1. Finally, at vector distance calculation step, it is presented three different equations that can be applied: Euclidean norm (the original Rosenstein's approach) and other two alternative metrics, Spearman and Pearson distances. Moreover, the Caesarendra's algorithm described in Tab. 1 represents the subsequent steps to be followed for the LLE computation after initial distance matrix acquirement in Fig. 1.

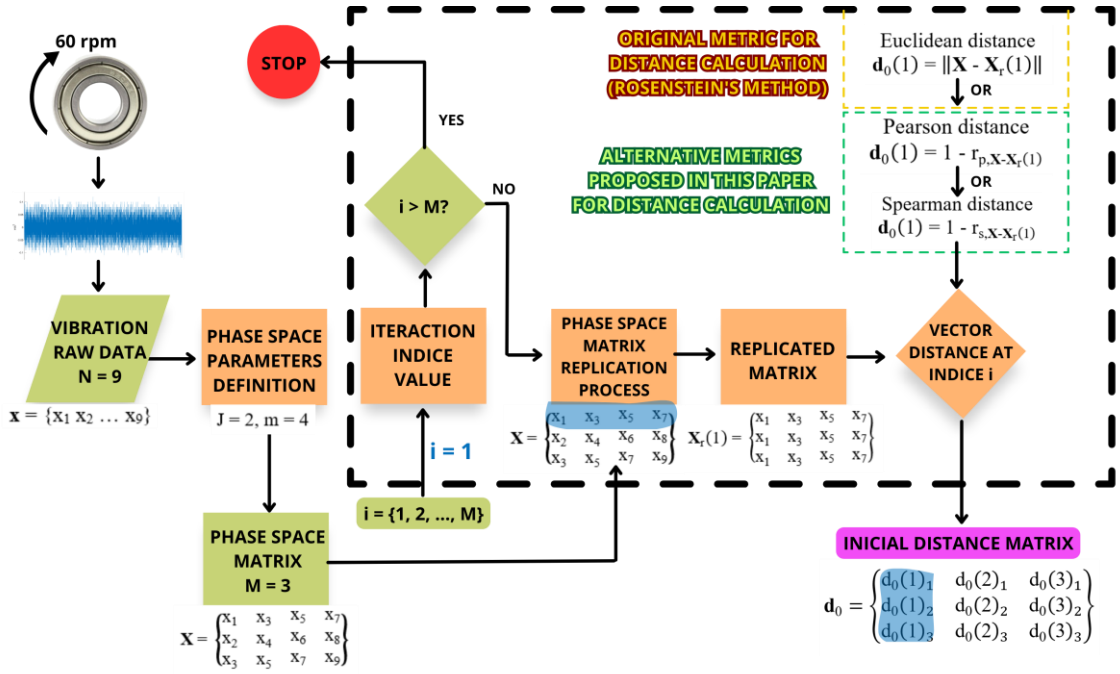

Figure 1. Flowchart describing the process to obtain the initial distance matrix.

Table 1. The algorithm proposed by Caesarendra et al. (2015) for calculation of LLE.

LLE calculation
$\boldsymbol{X}$ and $\boldsymbol{d}_0$ are calculated from Fig. 1
μ is the mean period calculated using Eq. 3
f_s is the sampling rate of the vibration signal
k_{max} is the maximum k-iteration limit of expansion range
Create the new matrix $\boldsymbol{d}_{0\_new}$. Then, set $\boldsymbol{d}_{0\_new} = \boldsymbol{d}_0$ initially.
for $i = 1$ **to** M **do**
for $j = 1$ **to** M **do**
if $\lvert j - i \rvert \leq \mu$ **then**
$\boldsymbol{d}_{0\_new}(j) = \max\lvert \boldsymbol{d}_0 \rvert$
end if
end for j
Find the minimum value $\Delta_a(i)$ of $d_{0\_new}(j)$ and its identifier index $\Delta_b(i)$:
$[\Delta_a(i), \Delta_b(i)] = \min\lvert d_{0\_new}(j) \rvert$
end for i
for $k = 1$ **to** k_{max} **do**
$bound = M - k$
$evolve = 0$
$point = 0$
for $h = 1$ **to** M **do**
if $h \leq bound$ **and** $\Delta_b(h) \leq bound$ **then**
$d = \sqrt{\sum[\boldsymbol{X}(h + (k-1), :) - \boldsymbol{X}(\Delta_b(h) + (k-1), :)]^2}$
if $d \neq 0$ **then**
$evolve = evolve + \ln\lvert d \rvert$
$point = point + 1$
end if
end if
end for h
if $point > 0$ **then**
$\boldsymbol{d}_{new}(k) = evolve/point$
else

33: $\boldsymbol{d}_{new}(k) = 0$
34: **end if**
35: **end for** k
36: Finally, find the angular coefficient α of the curve that fit $\boldsymbol{d}_{new}(k)$, then:
37: $LLE = \alpha f_s$

3. PEARSON AND SPEARMAN DISTANCES CALCULATION

The correlation between variables can be measured using several indices, which the three most popular are Pearson, Spearman and Kendall coefficients. Pearson's method was discovered by Bravais in 1846, but Karl Pearson was who in 1896 described the method more rigorously including some contributions, among which he proposed the normality of the analyzed variables. In briefly comments, Pearson's coefficient is a measure of the strength of the correlation between two quantitative variables. In 1904, facing with the problem of analyzing the correlation between qualitative variables, Spearman came up with the idea of adopting the same method as Pearson, however transforming the original variables into new ranked variables (Hauke and Kossowski, 2011).

The calculation of the correlation between two variables, according to Xiao et al. (2016), is based on how much a X variable can be used to predict the behavior of another variable Y, such that, $\hat{Y} = f(X)$. Where $\hat{Y}$ denotes the predicted values for Y based on a function of X. Thus, the accuracy of this prediction can be measured by the error between the actual value and the predicted value, i.e., $e = Y_i - \hat{Y}_i$. Thus, the mean squared error can be described as follows:

$$s_{yx}^2 = \frac{\sum_{i=1}^{N} e_i^2}{N} = \frac{\sum_{i=1}^{N} (Y_i - \hat{Y}_i)^2}{N}, \tag{5}$$

Where N corresponds to the size of the dataset. Now, in this sense, establishing $\bar{X}$ and $\bar{Y}$ as the means of each variable X_i and Y_i, where s_x^2 and s_y^2 represent their respective variances, the standard definition for correlation r calculation is given by Eq. 6.

$$r = \frac{\sum_{i=1}^{N} (X_i - \bar{X})(Y_i - \bar{Y})}{N s_x s_y}, \tag{6}$$

According to Mukaka (2012), the result can vary from -1 to $+1$, so that the positive sign indicates that if one variable grows the other also grows, or if one decreases the other also decreases. When the sign is negative, it means that when one variable increases the other decreases, and vice versa. Furthermore, the closer the r is to ± 1, then stronger is the correlation; while closer to 0, the correlation becomes weak. For Xiao et al. (2016), Pearson's correlation coefficient measures the intensity and direction of strictly linear relationships between variables. According to Mukaka (2012), the distribution must be normal, as extreme values can impair the accuracy of the results. Finally, Mukaka (2012) and Xiao et al. (2016) report that the Pearson coefficient r_p is equivalent to the ratio between the sample covariance of the variables and their respective deviations.

$$r_p = \frac{\sum_{i=1}^{N} (X_i - \bar{X})(Y_i - \bar{Y})}{\sqrt{\left(\sum_{i=1}^{N} (X_i - \bar{X})^2\right)\left(\sum_{i=1}^{N} (Y_i - \bar{Y})^2\right)}}, \tag{7}$$

On the other hand, according to Xiao et al. (2016), despite being a special case of Pearson's method, Spearman's correlation coefficient is non-parametric (it does not depend on the type of distribution) and it measures the intensity and direction of the monotonic relationship between the variables. The monotonic relationship between two variables concerns the continuity in the trend of growth or decrease, although not at the same rate. Chok (2010) and Song and Park (2020) represent the equation for calculating Spearman's correlation coefficient r_s as a special case of the equation seen for Pearson's method in Eq. 7, but this time based on X_i' and Y_i', which are the ranked random variables X_i and Y_i:

$$r_s = \frac{\sum_{i=1}^{N} (X_i' - \bar{X}')(Y_i' - \bar{Y}')}{\sqrt{\left(\sum_{i=1}^{N} (X_i' - \bar{X}')^2\right)\left(\sum_{i=1}^{N} (Y_i' - \bar{Y}')^2\right)}}, \tag{8}$$

Finally, according to Xie et al. (2016), the Pearson and Spearman distances can be calculated by the following relations, respectively:

$$d_p = 1 - r_p, \tag{9}$$

$$d_s = 1 - r_s, \tag{10}$$

4. *t*-WELCH STATISTIC VALUE ESTIMATION

According to Zimmerman and Zumbo (1993), in order to compare the means of two independent groups, the Welch's *t*-test is considered better than Student *t*-test when the populations don't have the same variance and size. Additionally, it is worth noting that when Welch's *t*-test is applied to groups with same variance and size, the result is equal to Student *t*-test. For this work, the groups were assumed to have unequal variances and follow a normal distribution. Thus, the statistical significance value for each calculated feature in order to evaluate their capability to maximize class separation is estimated by Eq. 11 of Welch's *t*-test statistic as following, where i and j correspond both groups evaluated, $\bar{x}$ corresponds to sample mean, σ^2 is sample variance and N is the sample length (Shri and Sriraam, 2017):

$$t = \frac{\bar{x}_i - \bar{x}_j}{\sqrt{\frac{{\sigma_i}^2}{N_i} + \frac{{\sigma_j}^2}{N_j}}}, \tag{11}$$

5. EXPERIMENTAL DATA AQUISITION

Figure 1 presents the test rig and the acquisition system utilized NK820 da Teknikao®. Upon (vertical) the bearing housing (yellow color) is the accelerometer NK30 43649 with sensitivity of 101 mV/g. Additionally, a WEG CFW08 frequency inverter was associated to a 3 hp three-phase induction motor AC with 3 poles, but the pulley at the extremity of the shaft was no longer used during the tests. Furthermore, Tab. 2 shows the parameters set to data acquisition, where "D" means "dataset". There are three datasets obtained at shaft speed of 60 rpm. The main difference between them is the frequency range and the sampling rate. Therefore, 250 observations were acquired for each dataset (D1, D2 and D3), 125 belong to a health bearing (normal) and 125 refer to a bearing with a simulated fault in outer race as soft scratches. Those both bearings tested were GBR 6202z.

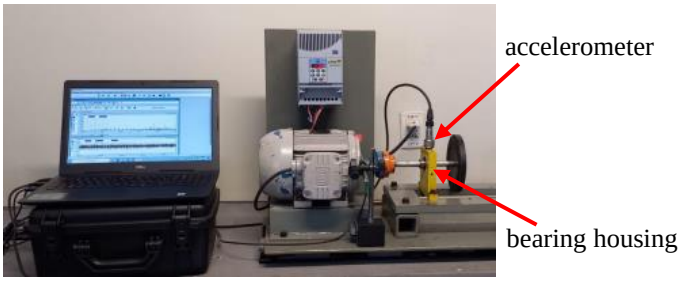

Figure 2. Test rig and acquisition system.

Table 2. Parameters adjusted for vibration signals acquisition.

Parameters	D1	D2	D3
Shaft speed (rpm)	60	60	60
Frequency range (Hz)	0.1 – 1000	0.1 – 2000	0.1 – 5000
Sampling rate (kHz)	2.5	5.0	12.5
Number of points	4096	8192	16384
Time step (ms)	0.4	0.2	0.08
Time period (s)	1.6380	1.6382	1.3106

6. RESULT AND DISCUSSION

For the calculation of the LLE based on the experimental vibration data used in this paper, as mentioned in section 2, it is needed to reconstruct the phase space subjecting the vibration signal to embedding theorem and adopting a suitable time delay. For time lag, $J = 1$ allowed to find a more satisfactory results, such as in Rosenstein et al. (1993). About the others parameters, the embedding dimension of the phase-space was defined as $m = 50$ after testing different values, the mean period is particular to each signal and it was calculated using Eq. 3. The Expansion Range was defined between $k_{min} = 1$ and $k_{max} = 50$ (where k_{max} must be between μ and m, according to Caesarendra et al. (2015)). The LLE was computed considering the three different distances metrics (Euclidean, Pearson and Spearman) at finding nearest point stage. Thus, Figure 3 shows the class separability significance of LLE calculated for dataset D1, D2 and D3.

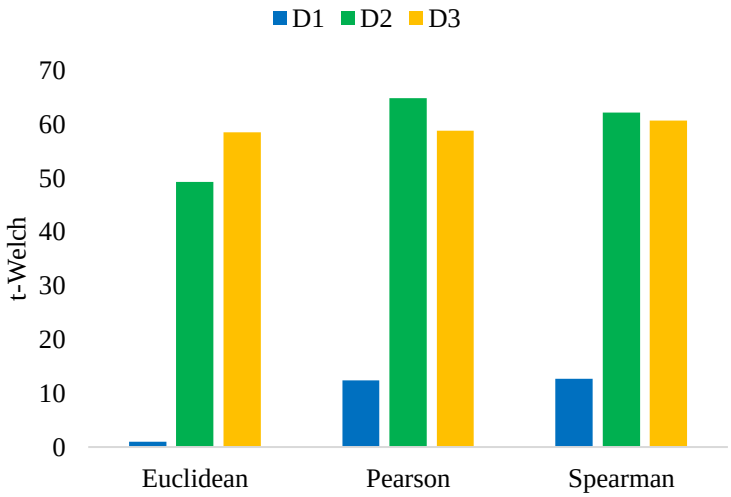

Figure 3. Ranking of significance class separation.

When Rosenstein, Collins and De Luca (1993) proposed their method for calculating the LLE, the authors emphasized that the quality of the results depends on the resolution of the time series. In fact, Figure 3 shows that the t-Welch significances were inferior for D1 due to its relatively low sampling rate compared to datasets D2 and D3. Anyway, Figure 2 also presents that the use of Pearson or Spearman distance in step of finding nearest neighbors can improve class separation, especially for dataset D1. Hence, the proposed changing in Rosenstein's algorithm seems to enhance class separation specifically for time series with lower resolution. The reason why this happens is difficult to visualize in the state space due to its high dimensional of 50 coordinates (embedding dimension). However, due to Pearson and Spearman distance consider the sample mean of each vector, it maybe makes the step of finding neighboring point more robust to noise, reducing the possibility of selecting a noisy point as the nearest point, which can affect the exponential behavior of the trajectories. Finally, Figure 4 shows the histograms that represent the binary distributions based on relative probability normalization per bin. Figure 3 analysis is supplemented by Fig. 4, since that showing the actual class distributions, allowing clearer observation of the impact of the proposed method in class separation.

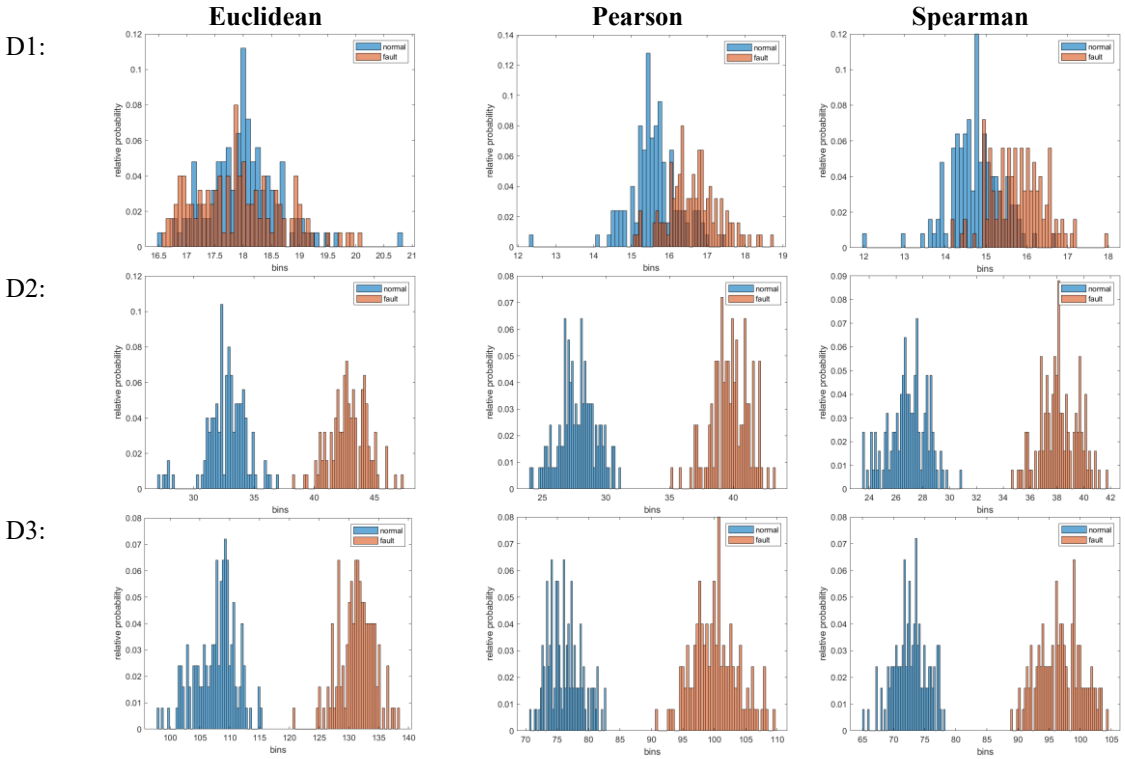

Figure 4. Histograms representing the probabilistic distributions of classes.

Two other sets of data were used to verify the proposed methodology, which were collected from belt conveyor pulleys operating in mining yard. First, a tail pulley (TP) rotating at 60 rpm and, subsequently, a snub pulley (SP) rotating at 83 rpm; furthermore, the bearing of each pulley had outer race degraded. The two vibration datasets were collected at a sampling rate of 2048 Hz, frequency range of 0.1 Hz – 1 kHz and time period of 1 s. The dataset TP has 300 samples of healthy bearing and 1168 samples of faulty bearing. The SP, on the other hand, has 568 and 604, respectively. The results also showed an increase in class separability, similarly observed in the laboratory tests discussed above.

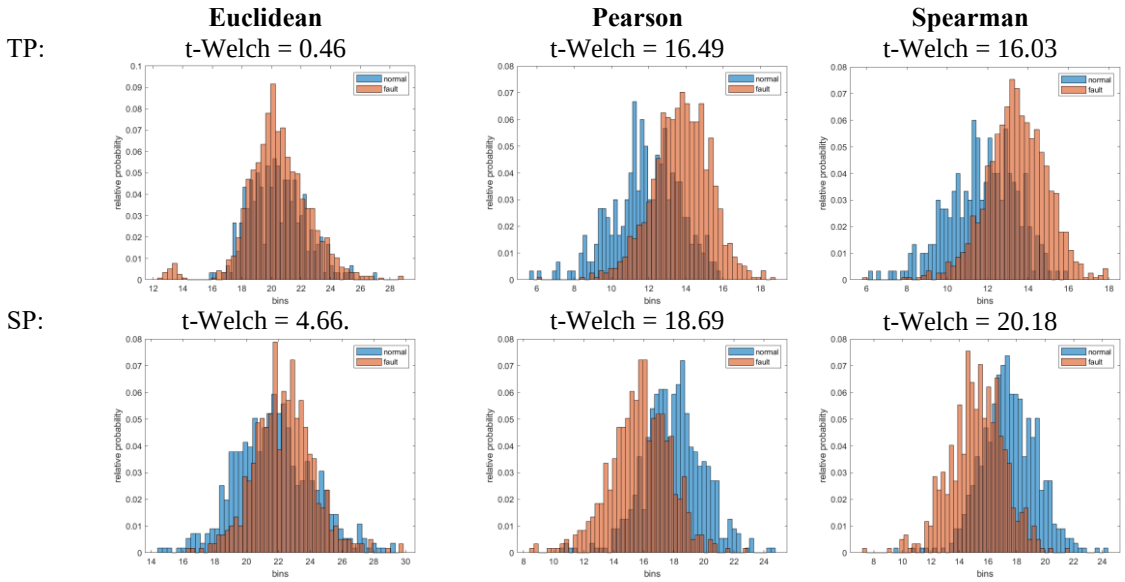

7. CONCLUSION

This paper evaluated the impact of adopting different metrics (Pearson and Spearman distances) at finding neighboring points step of the LLE calculation algorithm proposed by Rosenstein (which is originally based on Euclidean distance). The experimental vibration data used for the current method's validation consists of three datasets distinguished by acquisition parameters such as sampling rate and frequency range, which affect the resolution of the time series. Generally, one of the drawbacks of vibration signals with high resolutions is the storage cost, then storing a large amount of high-resolution vibration data for prognosis approaches becomes a shortcoming issue. However, the results showed the LLE calculation based on either Spearman or Pearson metrics can improve class separation even when low-resolution time series was utilized. Thus, despite of high-resolution time series be recommended for accurate LLE estimation, the alternative metrics proposed in this paper can also found improved results for low-resolution data.

Moreover, the class separation measured by *t*-Welch statistic value showed that the changing proposed in this paper just made difference the lower the time series resolution, in other words, for the highest resolution data, the use of alternative metrics did not present a significance alteration. Thus, the LLE calculation with alternative metrics showed to be more robust to noise, probably due to each state vector being centered at its own sample mean in both Pearson and Spearman equations. Hence, increasing the separability significance of LLE based on Pearson or Spearman turn the LLE a more reliable predictor for diagnosis tasks through machine learning classification algorithms, which can become more generalized. Furthermore, the results using either Pearson or Spearman norms presented equivalent results, allowing to adopt any of both, since their fundamental mathematic is similar. Finally, this work shows how much sensitive the Rosenstein's LLE algorithm can be, and raises a question about the possibility of existence of another better metric or even another method to find the neighboring points in state space.

8. ACKNOWLEDGEMENTS

We thank Dynamox for all the support and funding.

9. REFERENCES

Awrejcewicz, J., Krysko, A., Pavlov, S., Zhigalov, M., and Krysko, V., 2017, Chaotic dynamics of size dependent Timoshenko beams with functionally graded properties along their thickness, Mechanical Systems and Signal Processing, Vol. 93, pp. 415-430.

Caesarendra, W., Kosasih, B., Tieu, A., and Moodie, C., 2015, Application of the largest Lyapunov exponent algorithm for feature extraction in low-speed slew bearing condition monitoring, Mechanical Systems and Signal Processing, Vol. 50-51, pp. 116-138.

Chok, N. S., 2010. *Pearson's versus Spearman's and Kendall's correlation coefficients for continuous data*. Ph.D. thesis, University of Pittsburgh, Russia.

Ghafari, S., Golnaraghi, F., and Ismail, F., 2008, Effect of localized faults on chaotic vibration of rolling element bearings, Nonlinear Dynamics, Vol. 53, No. 4, pp. 287-301.

Hauke, J., and Kossowski, T., 2011, Comparison of values of Pearson's and Spearman's correlation coefficients on the same sets of data, Quaestiones geographicae, Vol. 30, No. 2, p. 87.

Mehdizadeh, S., 2019, A robust method to estimate the largest Lyapunov exponent of noisy signals: A revision to the Rosenstein's algorithm, Journal of Biomechanics, Vol. 85, pp. 84-91.

Mehdizadeh, S., and Sanjari, M. A., 2017, Effect of noise and filtering on largest Lyapunov exponent of time series associated with human walking, Journal of biomechanics, Vol. 64, pp. 236-239.

Mukaka, M. J. M. M. J., 2012, Statistics corner: a guide to appropriate use of correlation in medical research, Malawi Med J, Vol. 24, No. 3, pp. 69-71.

Ogunjo, S., Fuwape, I., & Temiye, M., 2021, Impact of global financial crisis on the complexity of emerging markets: Case study of the Nigerian Stock Exchange, Pramāṇa – J Phys, Vol. 95, p. 206.

Patel, V., Tandon, N., and Pandey, R., 2012, Defect detection in deep groove ball bearing in presence of external vibration using envelope analysis and Duffing oscillator. Measurement: Journal of the International Measurement Confederation, Vol. 45, No. 5, pp. 960-970.

Qingjun, G., and Yang, L., 2019, Early Fault Diagnosis of Rolling Bearing Based on Lyapunov Exponent, Journal of Physics, Conference Series, Vol. 1187, No. 3, p. 32073.

Raffalt, P., Kent, J., Wurdeman, S., & Stergiou, N., 2019, Selection Procedures for the Largest Lyapunov Exponent in Gait Biomechanics, Annals of Biomedical Engineering, Vo. 47, No. 4, pp. 913-923.

Rai, A., and Kim, J., 2020, A novel health indicator based on the Lyapunov exponent, a probabilistic self-organizing map, and the Gini-Simpson index for calculating the RUL of bearings, Measurement: Journal of the International Measurement Confederation, Vol. 164, p. 108002.

Rosenstein, M., Collins, J., and De Luca, C., 1993, A practical method for calculating largest Lyapunov exponents from small data sets, Physica. D, Vol. 65 No. 1, pp. 117-134.

Shri, T. P., and Sriraam, N., 2017, Comparison of t-test ranking with PCA and SEPCOR feature selection for wake and stage 1 sleep pattern recognition in multichannel electroencephalograms, Biomedical Signal Processing and Control, Vol. 31, pp. 499-512.

Soleimani, A., and Khadem, S., 2015, Early fault detection of rotating machinery through chaotic vibration feature extraction of experimental data sets, Chaos, Solitons and Fractals, Vol. 78, pp. 61-75.

Song, H. Y., and Park, S., 2020, An analysis of correlation between personality and visiting place using Spearman's rank correlation coefficient, KSII Transactions on Internet and Information Systems (TIIS), v. 14, n. 5, p. 1951-1966.

Takens, F., 1981, Detecting strange attractors in turbulence, Dynamical Systems and Turbulence, Vol. 898, p. 366.

Tao Xinmin, Du Baoxiang, and Xu Yong., 2007. "Bearings Fault Diagnosis based on GMM Model using Lyapunov Exponent Spectrum". In *IECON 2007 - 33rd Annual Conference of the IEEE Industrial Electronics Society*, Taipei, Taiwan, pp. 2666-2671.

Tayel, M., & AlSaba, E., 2015, Robust and Sensitive Method of Lyapunov Exponent for Heart Rate Variability, ArXiv, Vol. abs/1508.00996, p. 19.

Wang, F., Liu, C., Su, W., Xue, Z., Han, Q., and Li, H., 2018, Combined Failure Diagnosis of Slewing Bearings Based on MCKD-CEEMD-ApEn, Shock and Vibration, Vol. 2018, pp. 1-13.

Xiao, C., Ye, J., Esteves, R. M., and Rong, C., 2016, Using Spearman's correlation coefficients for exploratory data analysis on big dataset. Concurrency and Computation: Practice and Experience, Vol. 28, No. 14, pp. 3866-3878.

Xie, Y., Wang, Y., Nallanathan, A., and Wang, L., 2016, An improved K-nearest-neighbor indoor localization method based on spearman distance, IEEE signal processing letters, Vol. 23, No. 3, p. 351-355.

Yakovleva, T., Kutepov, I., Karas, A., Yakovlev, N., Dobriyan, V., Papkova, I., . . . Krysko, V., 2020, EEG Analysis in Structural Focal Epilepsy Using the Methods of Nonlinear Dynamics (Lyapunov Exponents, Lempel–Ziv Complexity, and Multiscale Entropy), The Scientific World Journal, Vol. 2020, p. 13.

Yousuf, L., 2019, Experimental and simulation investigation of nonlinear dynamic behavior of a polydyne cam and roller follower mechanism, Mechanical Systems and Signal Processing, Vol. 116, pp. 293-309.

Zimmerman, D. W., and Zumbo, B. D., 1993, Rank transformations and the power of the Student *t*-test and Welch t-test for non-normal populations with unequal variances, Canadian Journal of Experimental Psychology, Vol. 47, No. 3, pp. 523–539.

10. RESPONSIBILITY NOTICE

The authors are the only responsible for the printed material included in this paper.